Computational Materials Science 56 (2012) 11–17

Contents lists available at SciVerse ScienceDirect

Computational Materials Science

journal homepage: www.elsevier.com/locate/commatsci

# Mechanical properties of the hexagonal boron nitride monolayer: *Ab initio* study

Qing Peng *, Wei Ji, Suvranu De

*Department of Mechanical, Aerospace and Nuclear Engineering, Rensselaer Polytechnic Institute, Troy, NY 12180, USA*

ARTICLE INFO

*Article history:*
Received 27 October 2011
Received in revised form 23 December 2011
Accepted 27 December 2011
Available online 25 January 2012

*Keywords:*
Hexagonal boron nitride monolayer
Density functional theory
Fifth-order elastic constants
Non-linear elastic properties

ABSTRACT

Using density functional theory (DFT) calculations we found that hexagonal boron nitride monolayer (h-BN) shows a non-linear elastic deformation up to an ultimate strength followed by a strain softening to the failure. To develop a continuum based model for such non-linear behavior, we proposed a method to study high order elastic constants of the 2D hexagonal structures. The continuum description of the elastic properties of monolayer h-BN is obtained using this method through *ab initio* density functional theory. This rigorous continuum description of the elastic response is formulated by expanding the elastic strain energy density in a Taylor series in strain truncated after the fifth-order term. we obtained a total of fourteen non-zero independent elastic constants for up to tenth-order tensor.



## 1. Introduction

The research on 2D nanomaterials with potential next generation electronic device application has seen tremendous progress in the past few years. An example of such nanostructures is hexagonal boron nitride (h-BN) monolayer which is analog of graphene having a honeycomb lattice structure [28]. Hexagonal boron nitride is chemically inert, has a high thermal conductivity, and is highly temperature resistant to oxidation. Due to its outstanding properties, h-BN has found wide applications in micro and nano-devices such as insulator with high thermal conductivity in electronic devices [28], ultraviolet-light emitter in optoelectronics [10,32,15,1,35], and as nano-fillers in high strength and thermal conductive nanocomposites [23,38]. In very recent works, it has been shown that a tunable band gap nanosheet can be constructed by fabrication of hybrid nanostructures made of graphene/h-BN domains, and this opens a new venue for huge research in the application of h-BN for electronics [8,5].

Given the aforementioned potential applications, the complete knowledge of mechanical and physical properties of h-BN monolayer, however, is still lacking. For example, the non-linear elastic mechanical properties have not been addressed yet, although previous works have reported that the h-BN monolayer has a bulk modulus around 160 GPa and a bending modulus around 31.2 GPa (Refs. [28,24,9,33]). Several experimental and atomistic simulation studies, on graphene and carbon nanotubes, have probed that 2D nanosheets and nanotubes usually show a non-linear elastic deformation during the tension up to the intrinsic strength of the material followed by a strain softening up to the fracture [22,25,37,14,27]. To establish a continuum based framework to capture this non-linear elastic behavior of the 2D nanosheets, the higher order elastic constants must be considered in the strain energy density function [4,36]. In such a model, the strain energy density is expanded in a Taylor series to include both quadratic as well as higher order terms in strain. The quadratic term accounts for the linear elastic response of the material while the cubic and higher order terms account the strain softening of the elastic stiffness. The higher order terms also can be used to define other anharmonic properties of this 2D nanostructure including phenomena such as thermal expansion, phonon–phonon interaction, etc. [11].

The goal of this paper is to introduce a method to obtain an accurate continuum description of the elastic properties of a general 2D hexagonal structure such as monolayer h-BN, from *ab initio* density functional theory calculations. This continuum description is suitable for incorporation into the finite element method. As a result, this method could also very useful for multiscale calculations passing electronic scale information about mechanical properties to continuum level. To achieve that, we first examined the elastic properties of the h-BN monolayer using *ab initio* density functional theory. We adopted a fifth-order series expansion of the strain energy density function in order to model the in-plane elastic properties of h-BN.

Under the frame work of quantum mechanics, the DFT calculations can predict the elastic properties of materials if one takes into account the structural relaxations along with gradient corrections [31]. It was demonstrated that the resulting continuum description is capable to describe those accompanying *ab initio* DFT calculations with high accuracy in the infinitesimal strain regime as well as at finite strains, including the strain at the intrinsic stress and

* Corresponding author. Address: 110 8th Street, JEC 2303, Troy, NY 12180, USA. Tel.: +1 518 279 6669; fax: +1 518 276 6025.
*E-mail address:* qpeng.org@gmail.com (Q. Peng).
*URL:* http://qpeng.org (Q. Peng).

0927-0256/$ - see front matter © 2011 Elsevier B.V. All rights reserved.
doi:10.1016/j.commatsci.2011.12.029

beyond in graphene [36]. A higher rank tensor is associated with each term of the series expansion and the components of the tensor represent the continuum elastic properties. Previous authors had determined the non-zero independent tensor components that correspond to the symmetry elements of graphene for the second-, third-, fourth- and fifth-order term from stress–strain response of graphene [36]. We extended the method with least-squares solution to over-determined (up to eighth-rank tensor) and well-determined (tenth-rank tensor) linear equations. This method is introduced in Section 2. We applied this method to obtain the continuum description of the elastic properties of monolayer h-BN. The details of the DFT calculations are presented in Section 3, followed by the results and discussions in the Section 4. The conclusions are in Section 5.

## 2. Nonlinear elasticity theory

Our method is an extension of the method introduced by Wei et al. [36]. Our improvement is the least-square solution to the over-determined (up to eighth-rank tensor) and well-determined (tenth-rank tensor) linear equations. We used a super cell containing 12 B and 12 N atoms in one plane, with periodic boundary conditions. The undeformed reference configuration is shown in Fig. 1, with lattice vectors $\mathbf{H}_i$, $i = 1, 2, 3$. When a macroscopically homogeneous deformation (deformation gradient tensor [6] $\mathbf{F}$) is applied, the lattice vectors of the deformed h-BN are $\mathbf{h}_i = \mathbf{F}\mathbf{H}_i$. The Lagrangian strain [3] is defined as $\boldsymbol{\eta} = \frac{1}{2}(\mathbf{F}^{\mathbf{T}}\mathbf{F} - \mathbf{I})$, where $\mathbf{I}$ is the identity tensor. The strain energy density has functional form of $\boldsymbol{\Phi} = \boldsymbol{\Phi}(\boldsymbol{\eta})$. The elastic properties of a material are determined from $\boldsymbol{\Phi}$, which is quadratic in strain for a linear elastic material. Nonlinear elastic constitutive behavior is established by expanding $\boldsymbol{\Phi}$ in a Taylor series in terms of powers of strain $\boldsymbol{\eta}$. The symmetric second Piola–Kirchhoff stress tensor, $\Sigma_{ij}$, can be expressed (up to fifth order) as [36]:

$$\begin{aligned}\Sigma_{ij} &= \frac{\partial \Phi}{\partial \eta_{ij}} \\ &= C_{ijkl}\eta_{kl} + \frac{1}{2!}C_{ijklmn}\eta_{kl}\eta_{mn} + \frac{1}{3!}C_{ijklmnop}\eta_{kl}\eta_{mn}\eta_{op} \\ &\quad + \frac{1}{4!}C_{ijklmnopqr}\eta_{kl}\eta_{mn}\eta_{op}\eta_{qr}. \end{aligned} \tag{1}$$

where $\eta_{ij}$ is Lagrangian elastic strain. Summation convention is employed for repeating indices; lower case subscripts range from 1 to 3. Herein $\mathbf{C}$ denotes each higher-order elastic modulus tensor; the rank of each tensor corresponds to the number of subscripts. The second-order elastic constants (SOEC), $C_{ijkl}$, third-order elastic constants (TOEC), $C_{ijklmn}$, fourth-order elastic constants (FOEC), $C_{ijklmnop}$, and fifth-order elastic constants (FFOEC), $C_{ijklmnopqr}$, are given by the components of the fourth-, sixth-, eighth-, and tenth-rank tensors, respectively.

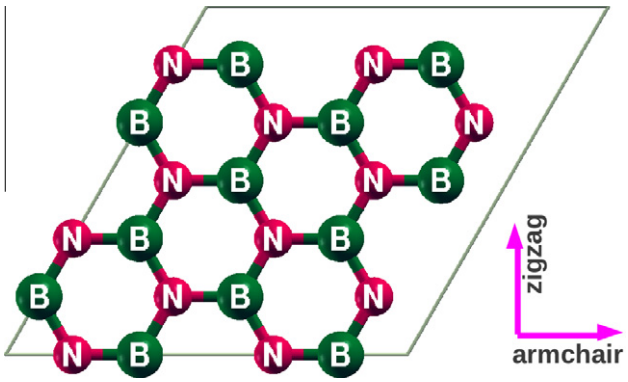


**Fig. 1.** Atomic super cell (24 atoms) of h-BN in the undeformed reference configuration.

We used conventional Voigt notation [29] for subscripts: $11 \to 1$, $22 \to 2$, $33 \to 3$, $23 \to 4$, $31 \to 5$, and $12 \to 6$. It should be mentioned that for strain $\eta_4 = 2\eta_{23}$, $\eta_5 = 2\eta_{31}$, $\eta_6 = 2\eta_{12}$. Eq. (1) can be rewritten as

$$\begin{aligned}\Sigma_I &= \frac{\partial \Phi}{\partial \eta_I} = C_{IJ}\eta_J + \frac{1}{2!}C_{IJK}\eta_J\eta_K + \frac{1}{3!}C_{IJKL}\eta_J\eta_K\eta_L \\ &\quad + \frac{1}{4!}C_{IJKLM}\eta_J\eta_K\eta_L\eta_M. \end{aligned} \tag{2}$$

where the summation convention for upper case subscripts runs from 1 to 6. These constants are orientation-independent in h-BN due to the sixfold rotation symmetry of the atomic lattice [29].

In this study, we modeled the monolayer h-BN as two dimensional (2D) structure and assume that the deformed state of the monolayer h-BN is such that the contribution of bending to the strain energy density is negligible as compared to the in-plane strain contribution. This assumption is reasonable since the radius of curvature of out-of-plane deformation are significantly larger than the in-plane inter-atomic distance. Then the stress state of monolayer h-BN under those assumptions can be assumed to be 2D and we only consider the in-plane stress and strain components for these kind of structures.

The components of the TOEC, FOEC, and FFOEC tensors can be determined based on the symmetries of the graphene atomic lattice point group $D_{6h}$ which consists of a sixfold rotational axis and six mirror planes as formulated in ref [36].

The fourteen independent elastic constants of h-BN are determined by a least-square fit to stress–strain results from *ab initio* DFT simulations in two steps. At the first step, we use least-squares fit to five stress–strain responses. Five relationships between stresses and strains are necessary because there are five independent FFOECs. We obtain the stress–strain relationships by simulating the following deformation states: uni-axial strain in the zigzag direction; uni-axial strain in the armchair direction; and, equibiaxial strain. From the first step, we find that the components of SOEC, TOEC, FOEC are over-determined (i.e, the number of linearly independent variables are greater than the number of constrains), and the FFOEC are well-determined (the number of linearly independent variables are equal to the number of constrains). Under such circumstance, the second step would be the least-square solution to these over- and well- determined linear equations.

At the first step, we carried out three deformations, uniaxial strain in the zigzag direction (case $z$), uniaxial strain in the armchair direction (case $a$) and equibiaxial strains (case $b$). For uniaxial strain in the zigzag direction, the strain tensor is,

$$\eta_{ij}^{z} = \begin{bmatrix} 0 & 0 & 0 \\ 0 & \eta_z & 0 \\ 0 & 0 & 0 \end{bmatrix}, \tag{3}$$

where $\eta_z$ is the amount of strain in zigzag direction.

For a given strain tensor, the associated deformation gradient tensor is not unique. The various possible solutions differing from one to another by a rigid rotation. Here the lack of a one-to-one map relationship between the strain tensor and deformation gradient tensor is not concerned since the calculated energy is invariant under rigid deformation [39,34]. One of the corresponding deformation gradient tensor $\mathbf{F}_z$ for uniaxial strain in the zigzag direction is selected as

$$\mathbf{F}_z = \begin{bmatrix} 1 & 0 & 0 \\ 0 & \varepsilon_z & 0 \\ 0 & 0 & 1 \end{bmatrix}, \tag{4}$$

where $\varepsilon_z$ is the stretch ration $\varepsilon$ in the zigzag direction. $\varepsilon$ is determined by the Lagrangian elastic strain through equation

$$\frac{1}{2}\varepsilon^2+\varepsilon-\eta=0. \tag{5}$$

The stress–strain relationships of the uniaxial strain in the zigzag direction are

$$\Sigma_1^z=C_{12}\eta_z+\frac{1}{2}C_{112}\eta_z^2+\frac{1}{6}C_{1112}\eta_z^3+\frac{1}{24}C_{11112}\eta_z^4, \tag{6}$$

$$\Sigma_2^z=C_{11}\eta_z+\frac{1}{2}C_{111}\eta_z^2+\frac{1}{6}C_{1111}\eta_z^3+\frac{1}{24}C_{11111}\eta_z^4, \tag{7}$$

For uniaxial strain in the armchair direction, the strain tensor is,

$$\eta_{ij}^a=\begin{bmatrix}\eta_a & 0 & 0\\ 0 & 0 & 0\\ 0 & 0 & 0\end{bmatrix}, \tag{8}$$

One of the corresponding deformation gradient tensor $\mathbf{F}_a$ for uniaxial strain in the armchair direction is

$$\mathbf{F}_a=\begin{bmatrix}\varepsilon_a & 0 & 0\\ 0 & 1 & 0\\ 0 & 0 & 1\end{bmatrix}, \tag{9}$$

where $\varepsilon_a$ is $\varepsilon$ in the armchair direction. The stress–strain relationships are

$$\Sigma_1^a=C_{11}\eta_a+\frac{1}{2}C_{222}\eta_a^2+\frac{1}{6}C_{2222}\eta_a^3+\frac{1}{24}C_{22222}\eta_a^4, \tag{10}$$

$$\Sigma_2^a=C_{12}\eta_a+\frac{1}{2}(C_{111}-C_{222}+C_{112})\eta_a^2+\frac{1}{12}(C_{1111}+2C_{1112}-C_{2222})\eta_a^3+\frac{1}{24}C_{12222}\eta_a^4, \tag{11}$$

For equibiaxial strain in-plane, $\eta_a=\eta_z=\eta$, the strain tensor is,

$$\eta_{ij}^b=\begin{bmatrix}\eta & 0 & 0\\ 0 & \eta & 0\\ 0 & 0 & 0\end{bmatrix}, \tag{12}$$

The corresponding deformation gradient tensor $\mathbf{F}_b$ for equibiaxial strain in-plane is

$$\mathbf{F}_b=\begin{bmatrix}\varepsilon & 0 & 0\\ 0 & \varepsilon & 0\\ 0 & 0 & 1\end{bmatrix}. \tag{13}$$

The stress–strain relationship is

$$\begin{aligned}\Sigma_1^b&=\Sigma_2^b\\ &=(C_{11}+C_{12})\eta+\frac{1}{2}(2C_{111}-C_{222}+3C_{112})\eta^2\\ &\quad+\frac{1}{6}\left(\frac{3}{2}C_{1111}+4C_{1112}+3C_{1122}-\frac{1}{2}C_{2222}\right)\eta^3+\frac{1}{24}\\ &\quad\times(3C_{11111}+10C_{11112}-5C_{12222}+10C_{1122}-2C_{22222})\eta^4.\end{aligned} \tag{14}$$

All fourteen elastic constants contribute to the expressions for stress–strain response for these three deformation states. But the components of SOEC, TOEC, FOEC are over-determined. As discussed before, we used least-squares solutions to solve the equations $\mathbf{A}\cdot\mathbf{C}=\mathbf{\Sigma}$ by computing the elastic constants that minimizes the Euclidean 2-norm $\|\mathbf{\Sigma}-\mathbf{A}\cdot\mathbf{C}\|^2$. For SOEC components, $C_{11}$, $C_{12}$ is obtained by

$$\begin{bmatrix}1 & 0\\ 0 & 1\\ 0 & 1\\ 1 & 0\\ 1 & 1\end{bmatrix}\begin{bmatrix}C_{11}\\ C_{12}\end{bmatrix}=\begin{bmatrix}\Sigma_2^z(O_1)\\ \Sigma_1^z(O_1)\\ \Sigma_2^a(O_1)\\ \Sigma_1^a(O_1)\\ \Sigma_1^b(O_1)\end{bmatrix} \tag{15}$$

where $\Sigma_1^z(O_1)$ is the coefficient of the first order of strain in $\Sigma_1^z$ (Eq. 9). Similar notation for the others. The Young's modulus is $E=\left(C_{11}^2-C_{12}^2\right)/C_{11}$ and Poisson's ratio is $\nu=C_{12}/C_{11}$.

For TOEC components $C_{111}$, $C_{112}$ and $C_{222}$ are obtained by

$$\frac{1}{2}\begin{bmatrix}1 & 0 & 0\\ 0 & 1 & 0\\ 1 & 1 & -1\\ 0 & 0 & 1\\ 2 & 3 & -1\end{bmatrix}\begin{bmatrix}C_{111}\\ C_{112}\\ C_{222}\end{bmatrix}=\begin{bmatrix}\Sigma_2^z(O_2)\\ \Sigma_1^z(O_2)\\ \Sigma_2^a(O_2)\\ \Sigma_1^a(O_2)\\ \Sigma_1^b(O_2)\end{bmatrix} \tag{16}$$

For FOEC components $C_{1111}$, $C_{1112}$, $C_{1122}$ and $C_{2222}$ are obtained by

$$\frac{1}{6}\begin{bmatrix}1 & 0 & 0 & 0\\ 0 & 1 & 0 & 0\\ 0.5 & 1 & 0 & -0.5\\ 0 & 0 & 0 & 1\\ 1.5 & 4 & 3 & -0.5\end{bmatrix}\begin{bmatrix}C_{1111}\\ C_{1112}\\ C_{1122}\\ C_{2222}\end{bmatrix}=\begin{bmatrix}\Sigma_2^z(O_3)\\ \Sigma_1^z(O_3)\\ \Sigma_2^a(O_3)\\ \Sigma_1^a(O_3)\\ \Sigma_1^b(O_3)\end{bmatrix} \tag{17}$$

For FFOEC components $C_{11111}$, $C_{11112}$, $C_{11122}$, $C_{12222}$ and $C_{22222}$ are obtained by

$$\frac{1}{24}\begin{bmatrix}1 & 1 & 0 & 0 & 0\\ 0 & 0 & 0 & 0 & 0\\ 0 & 0 & 0 & 1 & 0\\ 0 & 0 & 0 & 0 & 1\\ 3 & 10 & 10 & -5 & -2\end{bmatrix}\begin{bmatrix}C_{11111}\\ C_{11112}\\ C_{11122}\\ C_{12222}\\ C_{22222}\end{bmatrix}=\begin{bmatrix}\Sigma_2^z(O_4)\\ \Sigma_1^z(O_4)\\ \Sigma_2^a(O_4)\\ \Sigma_1^a(O_4)\\ \Sigma_1^b(O_4)\end{bmatrix} \tag{18}$$

With these fourteen independent elastic constants, the continuum formulation of h-BN up to fifth order can be obtained. This continuum formulation can present both linear and non-linear elastic mechanical properties in monolayer h-BN accurately from *ab initio* DFT calculations. As a result, this method can bridge up the scales in multiscale calculations passing electronic scale informations about mechanical properties to continuum level.

This method is good for a general 2D hexagonal structures due to the symmetries. It could be used for monolayer h-BNC heterostructures and other honeycomb-like structures.

## 3. Density-functional calculations

The stress–strain relationship of h-BN under the desired deformation configurations is characterized via *ab initio* calculations with the density-functional theory (DFT). DFT calculations were carried out with the Vienna Ab-initio Simulation Package (VASP) [17,20,19,18] which is based on the Kohn–Sham Density Functional Theory (KS-DFT) [12,16] with the generalized gradient approximations as parameterized by Perdew, Burke and Ernzerhof (PBE) for exchange–correlation functions [30]. The electrons explicitly included in the calculations are the ($2s^2 2p^1$) electrons of boron and ($2s^2 2p^3$) electrons of nitrogen. The core electrons ($1s^2$) of boron and nitrogen are replaced by the projector augmented wave (PAW) and pseudo-potential approach[2,13]. A plane-wave cutoff of 520 eV is used in all the calculations. The calculations are performed at zero temperature.

The criterion to stop the relaxation of the electronic degrees of freedom is set by total energy change to be smaller than 0.000001 eV. The optimized atomic geometry was achieved through minimizing Hellmann–Feynman forces acting on each atom until the maximum forces on the ions were smaller than 0.001 eV/Å.

The atomic structures of all the deformed and undeformed configurations are obtained by fully relaxing a 24-atom-unit cell where all atoms were placed in one plane. The simulation invokes

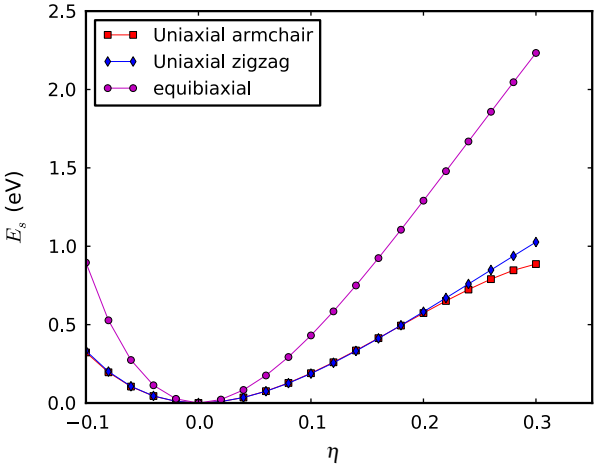


**Fig. 2.** Energy–strain responses for uniaxial strain in armchair and zigzag directions, and equibiaxial strains.

periodic boundary conditions for the two in-plane directions while the displacement to out-of-plane direction is forbidden.

The irreducible Brillouin Zone was sampled with a Gamma-centered $19 \times 19 \times 1$ $k$-mesh. Such large $k$-mesh was used to reduce the numerical errors caused by the strain of the systems. The initial charge densities were taken as a superposition of atomic charge densities. There was a 14 Å thick vacuum region to reduce the inter-layer interaction to model the single layer system. The results of the calculations are independent of the precise value of the out-of-plane thickness, so there is no physical interpretation attached to the quantity.

The VASP simulation calculates the true or Cauchy stresses, $\boldsymbol{\sigma}$, which for monolayer h-BN must be expressed as a 2D force per length with units of N/m by taking the product of the Cauchy stresses (with units of N/m$^2$) and the super-cell thickness of 14 Å. The Cauchy stresses are related to the second Piola–Kirchhoff (PK2) stresses $\boldsymbol{\Sigma}$ as

$$\boldsymbol{\Sigma} = J\mathbf{F}^{-1}\sigma(\mathbf{F}^{-1})^{T} \tag{19}$$

where $J$ is the determinant of the deformation gradient tensor $\mathbf{F}$.

## 4. Results and analysis

We first optimize the equilibrium lattice constant for monolayer h-BN. The total energy as a function of lattice spacing is obtained by specifying several lattice constants ($\sqrt{3}a_0$, where $a_0$ is B–N bond length) varying around 2.51 Å with full relaxations of all the atoms. A least-square fit of the energy vs. lattice constant with a fourth-order polynomial function yields the equilibrium lattice constant as 2.512 Å, which corresponds to the minimum total energy. The result is in good agreement with experiments[26] in h-BN (2.51 Å) This most energy favorite structure is set as the strain-free structure in this study and the geometry is shown in Fig. 1.

When the strains are applied, all the atoms are allowed full freedom of motion within plane. A quasi-Newton algorithm is used to relax all atoms into equilibrium positions within the deformed unit cell that yields the minimum total energy for the imposed strain state of the super cell.

Both compression and tension are considered here in order to sampling larger elastic deformation region. We studied the behavior of the system under the Lagrangian strain ranged from −0.1 to 0.3 with an increment of 0.02 in each step for all three cases. There are 63 *ab initio* DFT calculations in total.

The system's energy will increase when strains are applied. Here we define strain energy per atom $E_s = (E_{tot} - E_0)/n$, where $E_{tot}$ is the total energy of the strained system, $E_0$ is the total energy of the strain-free system, and $n$ is the number of atoms in the system. $E_s$ is a function of strain, in uniaxial armchair, uniaxial zigzag and equibiaxial deformation as shown in Fig. 2. $E_s$ responses differently at different strain direction, consistent to the non-isotropic structure of the monolayer h-BN. $E_s$ are non-symmetrical for compression ($\eta < 0$) and tension ($\eta > 0$) for all three cases. This non-symmetry indicates the anharmonicity of the monolayer h-BN structures. $E_s$ deviated from quadratic relationship with $\eta$ at strain of 0.04 in the three tested deformations.

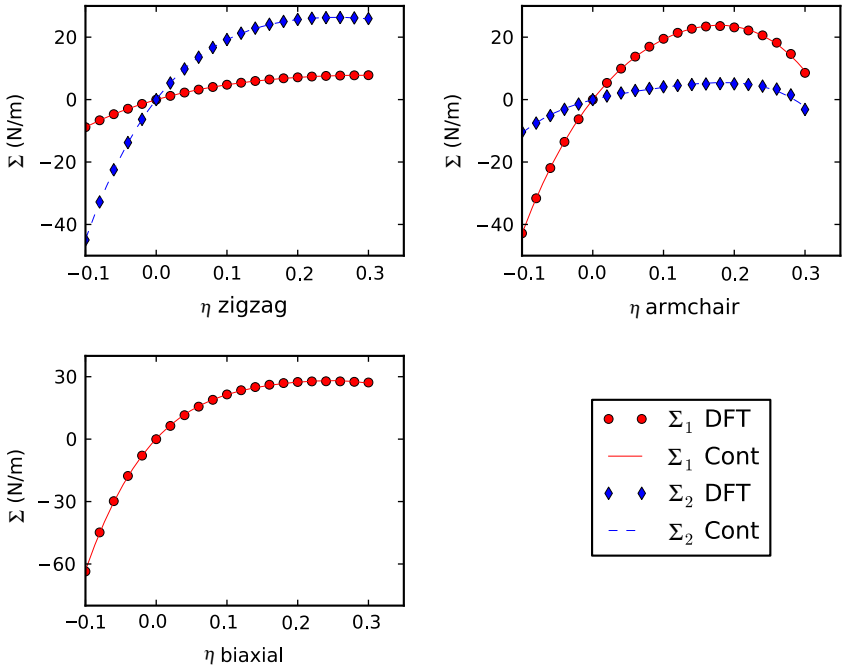


**Fig. 3.** Stress–strain responses for uniaxial strain in armchair and zigzag directions, and equibiaxial strains. The continuum responses are the least-square fit of the *ab initio* DFT calculations.

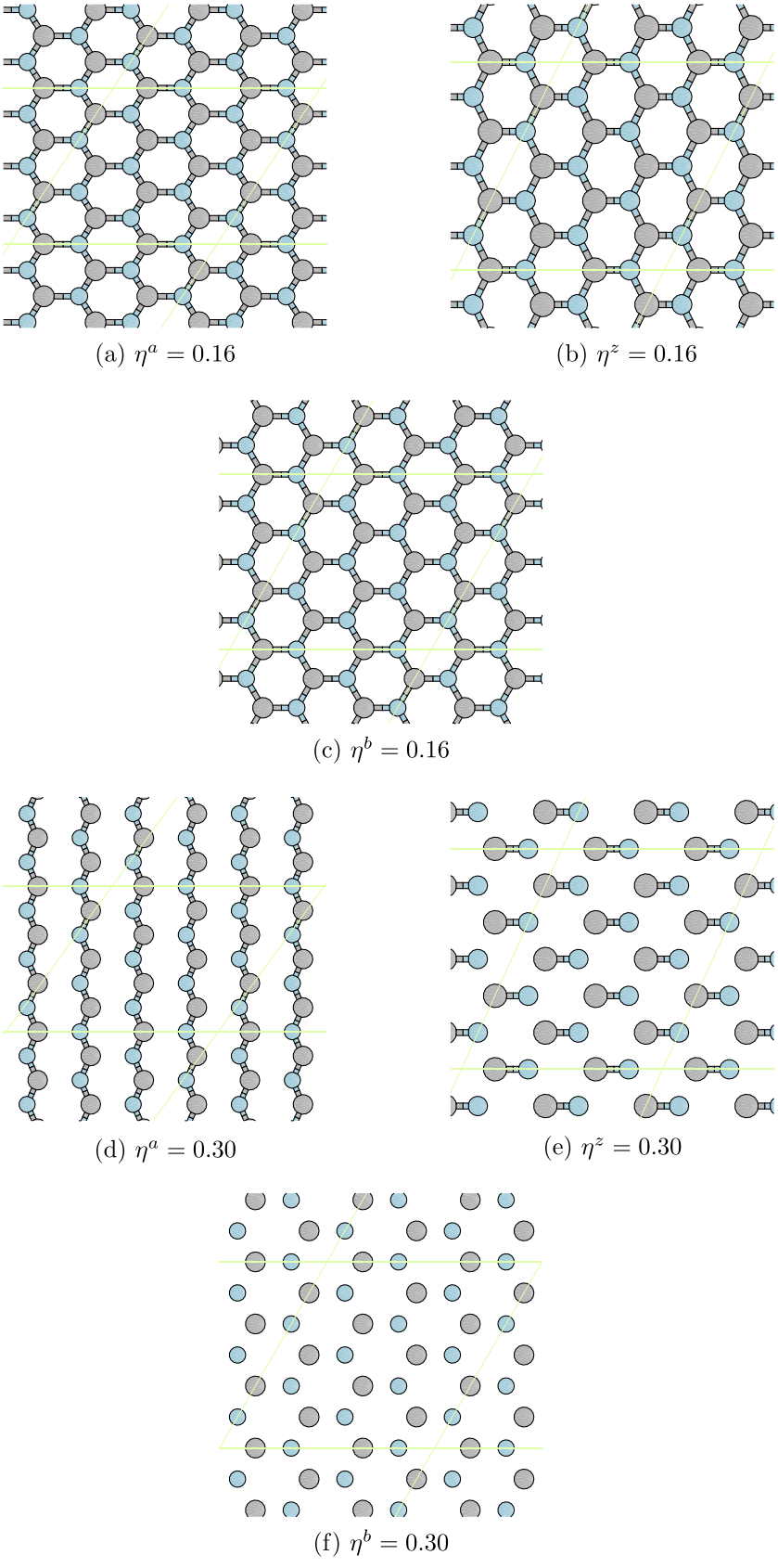


**Fig. 4.** The atomistic configurations of h-BN at the Lagrangian strain of 0.16 (a–c) and 0.30 (e–g). The larger and smaller circles represent B and N atoms,respectively.

The stress (second P–K stress) strain (Lagrangian strain) relationship for uniaxial strain in armchair and zigzag directions, and equibiaxial strains are shown in Fig. 3. These stress–strain curves reflect the fact of the non-isotropic h-BN structure and anharmonic response in compression and tension. For the uniaxial deformation along armchair direction, the maximum stresses are $\Sigma_1^a =$

**Table 1**
Nonzero independent components for the SOEC, TOEC, FOEC and FFOEC tensor components, Poisson's ratio $v$ and in-plane stiffness $Y_s$ of h-BN from DFT calculations.

| SOEC (N/m) | TOEC (N/m) | FOEC (N/m) | FFOEC (N/m) |
|---|---|---|---|
| $C_{11} = 293.2$ | $C_{111} = -2513.6$ | $C_{1111} = 16547$ | $C_{11111} = -65265$ |
| $C_{12} = 66.1$ | $C_{112} = -425.0$ | $C_{1112} = 2609$ | $C_{11112} = -8454$ |
| | $C_{222} = -2284.2$ | $C_{1122} = 2215$ | $C_{11122} = -28556$ |
| $Y_s = 278.3$ | | $C_{2222} = 12288$ | $C_{12222} = -36955$ |
| | | | $C_{22222} = -100469$ |

5.08, $\Sigma_1^a = 23.56$ (N/m) at $\eta_a = 0.18$. For the uniaxial deformation along armchair direction, the maximum stresses are $\Sigma_1^z = 26.26$ (N/m) at $\eta_z = 0.26$ and $\Sigma_2^z = 7.82$ (N/m) at $\eta_z = 0.30$. For the equibiaxial deformation, the maximum stresses are $\Sigma_1^b = \Sigma_2^b = 27.81$ (N/m) at $\eta = 0.24$.

The atomistic configurations at larger stain of 0.16 and 0.30 in these three deformation modes are presented in Fig. 4 for clarity. The B–N bonds along zigzag break first during the uniaxial zigzag deformation, as shown in Fig. 4.

The continuum responses are the least-square fit to the stress-stain results from the *ab initio* DFT calculations, as plotted in Fig. 3, by the Eqs. (6), (7), (10), (11) and (14). We then have 20 values for the fourteen independent elastic constants of h-BN from *ab initio* DFT calculations. The fourteen independent elastic constants of h-BN are finally determined by solving equations from Eqs. (15)–(18). The results of these fourteen independent elastic constants are grouped in SOEC, TOEC, FOEC and FFOEC and listed in Table 1. The in-plane Young's modulus $Y_s = 279.2$ (N/m) and Poison's ratio $v = 0.2176$ were obtained from $C_{11}$ and $C_{12}$. Our results of $C_{11}$, $C_{12}$, $Y_s$ and $v$ are comparable with *ab initio* prediction [21] and tight-binding calculations[10] of BN nanotubes.

Third-order elastic constants are important in understanding the non-linear elasticity of materials such as changes in acoustic velocities due to finite-strain. From Table 1, we can tell that TOECs and FFOECs are all negative while FOECs are positive. The h-BN monolayer shows an instability point under large tension. All stress–strain curves in previous section show that h-BN will soften when the strain is larger than an ideal strain. From the view of electron bonding, this is due to the bond tenuating and breaking. This softening behavior is determined by the TOECs and FFOECs in continuum aspect. The negative value of TOECs and FFOECs ensure the softening of h-BN under large strain beyond ideal strains.

The knowledge of these high order elastic constants is very useful to understand the anharmonicity. With the high order elastic constants, we can easily study the effect of the pressure $p$, acting on the plane of monolayer of h-BN sheet, on the second-order elastic moduli. Explicitly, while the pressure is applied, the second-order elastic moduli are transformed according to the relationships [29,7]:

$$\widetilde{C}_{11} = C_{11} - (C_{111} + C_{112})\frac{1-v}{Y_s}p, \tag{20}$$

$$\widetilde{C}_{22} = C_{11} - C_{222}\frac{1-v}{Y_s}p, \tag{21}$$

$$\widetilde{C}_{12} = C_{12} - C_{112}\frac{1-v}{Y_s}p. \tag{22}$$

The second-order elastic moduli increase linearly with the applied pressure $p$ within the third-order term truncation, as demonstrated in Fig. 5. When pressure is applied, the $\widetilde{C}_{11}$ is not symmetrical to $\widetilde{C}_{22}$ any more. Only when $p = 0$, $\widetilde{C}_{11} = \widetilde{C}_{22} = C_{11}$. This non-isotropy behavior could be the outcome of the anharmonicity.

These equations and plots also indicate that the h-BN monolayer responds differently under compression or tension along different directions.

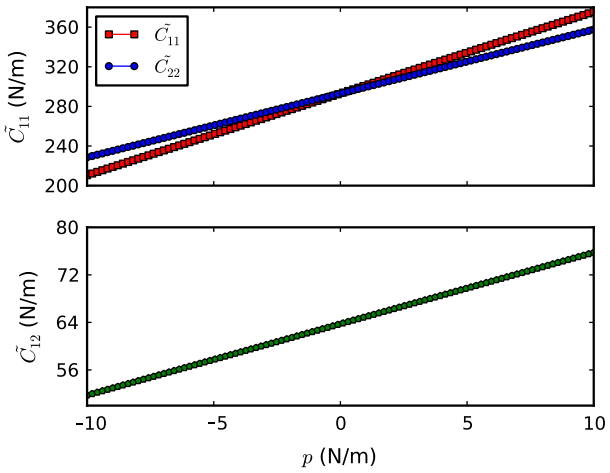


**Fig. 5.** Predicted second-order elastic moduli varies with the pressure $p$ acting in the plane of monolayer of h-BN sheet.

## 5. Conclusion

In summary, we proposed a method to obtain the continuum description of the elastic properties of monolayer h-BN through *ab initio* density functional theory. This thermodynamically rigorous continuum description of the elastic response is formulated by expanding the elastic strain energy density in a Taylor series in strain truncated after the fifth-order term. we obtained a total of fourteen non-zero independent elastic constants for up to the tenth-order tensor. We predicted the pressure dependent second-order elastic moduli. This continuum formulation is suitable for incorporation into the finite element method. Our method can bridge up the scales in multiscale calculations by passing electronic scale informations about mechanical properties to continuum level, in a general 2D hexagonal structures. The results of the DFT calculations for different deformation cases also revealed that the h-BN monolayer shows a non-linear elastic deformation up to an ultimate strength followed by a strain softening to the failure. The deformation and failure behavior, and the ultimate strength are highly anisotropic in these monolayers.

## Acknowledgements

The authors would like to acknowledge the generous financial support from the Defense Threat Reduction Agency (DTRA) Grant # BRBAA08-C-2-0130, U.S. Nuclear Regulatory Commission Faculty Development Program Grant # NRC-38-08-950 and U.S. Department of Energy (DOE) Nuclear Energy University Program (NEUP) Grant # DE-NE0000325.

## References

[1] X. Blase, A. Rubio, S.G. Louie, M.L. Cohen, Europhys. Lett. 28 (5) (1994) 335.
[2] P.E. Blöchl, Phys. Rev. B 50 (24) (1994) 17953–17979.
[3] K. Brugger, Phys. Rev. A 133 (6A) (1964) 1611.
[4] E. Cadelano, P.L. Palla, S. Giordano, L. Colombo, Phys. Rev. Lett. 102 (23) (2009) 235502.
[5] L. Ci, L. Song, C. Jin, D. Jariwala, D. Wu, Y. Li, A. Srivastava, Z.F. Wang, K. Storr, L. Balicas, F. Liu, P.M. Ajayan, Nature Mater. 9 (5) (2010) 430–435.
[6] M. Crisfield, Non-Linear Finite Element Analysis of Solids and Structures, John Wiley & Sons, New York, 1991.
[7] S.Y. Davydov, Phys. Solid State 53 (3) (2011) 665.
[8] G. Giovannetti, P.A. Khomyakov, G. Brocks, P.J. Kelly, J. van den Brink, Phys. Rev. B 76 (7) (2007) 073103.
[9] D. Golberg, Y. Bando, Y. Huang, T. Terao, M. Mitome, C. Tang, C. Zhi, ACS Nano 4 (6) (2010) 2979.
[10] E. Hernandez, C. Goze, P. Bernier, A. Rubio, Phys. Rev. Lett. 80 (20) (1998) 4502.
[11] Y. Hiki, Annu. Rev. Mater. Sci. 11 (1981) 51.
[12] P. Hohenberg, W. Kohn, Phys. Rev. 136 (3B) (1964) B864.

[13] R.O. Jones, O. Gunnarsson, Rev. Mod. Phys. 61 (3) (1989) 689–746.
[14] R. Khare, S.L. Mielke, J.T. Paci, S. Zhang, R. Ballarini, G.C. Schatz, T. Belytschko, Phys. Rev. B 75 (7) (2007) 075412.
[15] P. Kim, L. Shi, A. Majumdar, P.L. McEuen, Phys. Rev. Lett. 87 (21) (2001) 215502.
[16] W. Kohn, L.J. Sham, Phys. Rev. 140 (4A) (1965) A1133.
[17] G. Kresse, J. Hafner, Phys. Rev. B 47 (1993) 558.
[18] G. Kresse, J. Furthuller, Comput. Mater. Sci. 6 (1996) 15.
[19] G. Kresse, J. Furthuller, Phys. Rev. B 54 (1996) 11169.
[20] G. Kresse, J. Hafner, Phys. Rev. B 49 (1994) 14251.
[21] K.N. Kudin, G.E. Scuseria, B.I. Yakobson, Phys. Rev. B 64 (23) (2001) 235406.
[22] C. Lee, X. Wei, J.W. Kysar, J. Hone, Science 321 (5887) (2008) 385.
[23] G.W. Lee, M. Park, J. Kim, J.I. Lee, H.G. Yoon, Compos Part A – Appl Sci Manuf 37 (5) (2006) 727.
[24] C. Li, Y. Bando, C. Zhi, Y. Huang, D. Golberg, Nanotechnology 20 (38) (2009) 385707.
[25] F. Liu, P. Ming, J. Li, Phys. Rev. B 76 (6) (2007) 064120.
[26] L. Liu, Y.P. Feng, Z.X. Shen, Phys. Rev. B 68 (10) (2003) 104102.
[27] Q. Lu, R. Huang, Int. J. Appl. Mech. 1 (3) (2009) 443.
[28] A. Nag, K. Raidongia, K.P.S.S. Hembram, R. Datta, U.V. Waghmare, C.N.R. Rao, ACS Nano 4 (3) (2010) 1539.
[29] J.F. Nye, Physical Properties of Crystals, Oxford Science Publications, Oxford, 1995.
[30] J. Perdew, K. Burke, M. Ernzerhof, Phys. Rev. Lett. 77 (1996) 3865.
[31] P. Ravindran, R. Vidya, P. Vajeeston, A. Kjekshus, H. Fjellvag, J. Solid State Chem. 176 (2) (2003) 338.
[32] A.P. Suryavanshi, M.F. Yu, J.G. Wen, C.C. Tang, Y. Bando, Appl. Phys. Lett. 84 (14) (2004) 2527.
[33] M. Topsakal, E. Aktürk, S. Ciraci, Phys. Rev. B 79 (11) (2009) 115442.
[34] R. Wang, S. Wang, X. Wu, X. Liang, Phys. B – Cond. Matter 405 (16) (2010) 3501.
[35] K. Watanabe, T. Taniguchi, H. Kanda, Nature Mater. 3 (6) (2004) 404.
[36] X. Wei, B. Fragneaud, C.A. Marianetti, J.W. Kysar, Phys. Rev. B 80 (20) (2009) 205407.
[37] T. Xiao, X. Xu, K. Liao, J. Appl. Phys. 95 (12) (2004) 8145.
[38] C. Zhi, Y. Bando, C. Tang, H. Kuwahara, D. Golberg, Adv. Mater. 21 (28) (2009) 2889.
[39] J. Zhou, R. Huang, Internal lattice relaxation of single-layer graphene under in-plane deformation, J. Mech. Phys. Solids 56 (4) (2008) 1609.